Arabian Journal of Chemical and Environmental Research Vol. 12 Issue 2 (2025) 80–99



Effect of Pyrolysis Temperature on Characteristics and Adsorption of Pb(II) onto Millet Straw Derived Biochar from Aqueous Solution

I. Abubakar, M. D. Saeed and A.M Ayuba

Department of Pure and Industrial Chemistry, Bayero University PMB 3011, Kano, Nigeria.

Received 12 June 2025, Revised 18 July 2025 Accepted 22 July 2025

Cited as: I. Abubakar, M. D. Saeed and A.M Ayuba, Effect of Pyrolysis Temperature on Characteristics and Adsorption of Pb(II) onto Millet Straw Derived Biochar from Aqueous Solution, Arab. J. Chem. Environ. Res. 12(2), 80-99

Abstract

Millet straw was pyrolyzed to produce biochar for the removal of pollutants from water and to promote the resource utilization of agricultural waste. This study aimed to investigate the optimal preparation and adsorption conditions of millet straw-derived biochar and to explore its adsorption characteristics and mechanisms for Pb²⁺ removal from aqueous solutions. The effect of pyrolysis temperature on the physicochemical properties of the biochar was analyzed using scanning electron microscopy (SEM), Fourier-transform infrared spectroscopy (FTIR), X-ray diffraction (XRD), and Brunauer–Emmett–Teller (BET) surface area analysis. The optimum pyrolysis temperature was found to be 600 °C. The Langmuir isotherm and the pseudo-second-order kinetic model best described the adsorption equilibrium and kinetics, respectively. The maximum adsorption capacity predicted by the Langmuir model closely matched the experimental data. These findings suggest that millet straw biochar is an effective, low-cost adsorbent for the short-term removal of Pb²⁺ from contaminated water.

Keywords: Millet straw; Biochar; Physicochemical Properties; Adsorption; Lead.

1. Introduction

Heavy metals are widely recognized as hazardous to both human health and the environment due to their high toxicity (Machida *et al.*, 2019; Singh, Amit Kumar Dimitrios *et al.*, 2023). The increasing detection of heavy metals in various environmental compartments has become a serious global concern (Singh, Amit Kumar Dimitrios *et al.*, 2023; N. Zhang *et al.*, 2023). These metals are introduced into the environment primarily through improper disposal of industrial waste from mining, steel production, tanning, pigment synthesis, dye manufacturing, and petrochemical industries (Osman

ISSN : 2458-6544 $\ensuremath{\mathbb{O}}$ 2025 ; www.mocedes.org. All rights reserved.

^{*}Corresponding Author. E-mail address kainuwailiyas@gmail.com

et al., 2022). The U.S. Environmental Protection Agency (EPA) has classified lead (Pb) as a highly toxic, potentially carcinogenic metal. Prolonged exposure to lead can cause severe health problems, including nervous system disorders and cognitive impairment (Mahmoud et al., 2024; Osman et al., 2022). In this way, researchers have developed numerous biomaterials to remove heavy metals from wastewaters, thereby saving the environment and human life (Errich et al., 2021; El Hammari et al., 2022; Fouda-Mbanga et al., 2024; Meftah et al., 2025).

Biochar is a carbon-rich material produced by pyrolysis, a process that involves heating organic biomass, such as agricultural waste, wood chips, or manure, in a low-oxygen environment (J. Zhang *et al.*, 2014). It offers an environmentally sustainable method for managing organic waste, providing benefits for soil health, carbon sequestration, and environmental protection (Ren, 2014). In recent years, biochar has gained considerable attention as a low-cost and efficient adsorbent for the remediation of heavy metal-contaminated soils and wastewater (Feng *et al.*, 2023). The effectiveness of biochar in adsorption processes is attributed to its unique physicochemical properties, including its porous structure, abundant functional groups (such as carboxyl, carbonyl, and phenolic groups), large specific surface area (SSA), and the availability of low-cost biomass feedstocks for biochar production (Mahmoud *et al.*, 2024).

Although conventional materials, such as activated carbon and synthetic adsorbents, have been widely used for removing heavy metals, organic pollutants from wastewater, these methods are often expensive, less environmentally friendly, and unsuitable for large-scale applications (Kankou *et al.*, 2021; Pet *et al.*, 2024). Therefore, there is a pressing need to develop simple, efficient, and sustainable methods for lead (Pb) removal from wastewater (Zhou *et al.*, 2020).

In this study, millet straw, an abundant agricultural waste, was used to produce biochar through slow pyrolysis at four different temperatures. The physicochemical characteristics of the biochars were analyzed using various techniques, and batch adsorption experiments were performed to evaluate the Pb(II) adsorption capacity and removal efficiency of the biochar samples.

2.0.Methodology

2.1. Sample Collection and Preparation

Millet straw was utilized as the feedstock for biochar production in this study. The sampling was carried out during the rainy season, between July and August, from local farms in Kura Local Government Area of Kano State, Nigeria (approximately 11.7678° N latitude and 8.4263° E longitude) (Audu & Idowu, 2015). Fresh agricultural residues were randomly hand-picked from different locations within the sampling area, thoroughly mixed to form a composite sample, and subsequently packaged in clean, labelled polyethylene bags. The samples were then transported to the laboratory for further preparation

and analysis. Before the experiments, the collected millet straw feedstocks were thoroughly washed with distilled water to remove impurities. The samples were then air-dried for 30 days, after which they were cut into smaller pieces to facilitate uniform pyrolysis. Subsequently, the prepared samples were oven-dried using a thermostat oven (Model: DHG-9023A) at 105 °C for 24 hours to eliminate residual moisture prior to pyrolysis (Loc *et al.*, 2023).

2.2.Biochar Production

Biochar was generated according the procedure described by Alluqmani *et al.* (2019). The dried sample was placed in sealed crucibles and pyrolyzed in a tubular furnace (Carbolite Gero-30-30000, UK) at four different temperatures: 300, 400, 500, and 600 °C. Each temperature condition was maintained for 30, 60, 90, and 105 minutes, respectively at 10 °C/min. After pyrolysis, the samples were allowed to cool to room temperature inside a desiccator. The cooled biochar was ground, sieved to a particle size of 0.15 mm, and stored in airtight plastic containers for subsequent analyses. The biochar samples were labeled BCM300, BCM400, BCM500, and BCM600 based on their pyrolysis temperatures. Each pyrolysis was conducted in triplicate. The yield of biochar was calculated as the ratio of the produced biochar weight to the dry weight of original feedstock subjected to pyrolysis, using equation (1):

% Biochar Yeald =
$$\frac{\text{Mass of Biochar (g)}}{\text{Oven dry Mass of Feedstock}} X 100$$
 (1)

2.3. Biochar Characterization

2.3.1 Determination of pH

The pH of the biochar samples was determined using a 1:10 (w/v) biochar to deionized water (DW) ratio. The mixture was shaken on a reciprocating shaker at 37.5 °C for 1 hour. After shaking, the suspension was allowed to settle for 30 minutes. The pH of the supernatant was then measured using a pH meter (MIL170, Milwaukee, Italy) equipped with a calomel electrode—glass electrode system. Prior to measurement, the pH meter was calibrated with standard buffer solutions of pH 7 and pH 10, following the method described by Hu *et al* (Hu et al., 2022).

2.3.2 Electrical Conductivity

The electrical conductivity (EC) of the biochars was determined following the method described by *et al* (H. Liu et al., 2018)Biochar samples were mixed with deionized water at a 1:10 (w/v) ratio and shaken on a reciprocating shaker at 37.5 °C for 1 hour. The mixtures were then allowed to stand for 30 minutes to settle. The EC of the supernatant was subsequently measured using a pre-calibrated EC meter (MIL170, Milwaukee, Italy).

2.3.3 Determination of Cation Exchange Capacity (CEC)

Five grams (5 g) of each biochar sample were weighed into a 100 mL plastic beaker. Then, 40 mL of 1.0 mol/dm³ ammonium acetate solution (pH 7) was added. The mixture was stirred using a glass rod and left to stand overnight. The suspension was suction-filtered using a 55 mm Buchner funnel. The residue from the filtration was further leached with four successive 25 mL portions of 1.0 mol/dm³ NH₄Cl solution (pH 7). The combined solution was discarded, and the electrolyte was thoroughly washed out of the samples using 150 mL of ethanol. The sample was then allowed to drain completely. Subsequently, the sample was leached gradually with acidified NaCl solution to a final volume of 250 cm³. Into a 250 cm³ conical flask, 50 cm³ of 2% boric acid was measured, and 3 drops of a mixed indicator were added. The acidified NaCl leachate was transferred into a 500 cm³ Kjeldahl flask. To this, 10 cm of 1.0 M NaOH was added. The leachate was distilled, and the distillate was collected over the boric acid solution. The collected ammonium borate distillate was titrated with a standard 0.1 M HCl solution. The cation exchange capacity (CEC) was calculated using (2) equation (Y. Chen et al., 2018).

$$CEC (C mol kg^{1}) = \frac{VHClx MHCl x 1000}{\text{weight of sample}}$$
(2)

2.3.4 Determination of Point of Zero Charge (pHpzc)

The point of zero charge (pHpzc) of the biochar, which is the pH at which the net surface charge is zero, was determined using the solid addition method as described by *et al* (Yuan et al., 2024). In this method: 50 mL of 0.01 M NaCl solution was added into several 50 mL conical flasks. The initial pH of the solutions was adjusted within a range of 2–10 using 0.1 M NaOH or 0.1 M HCl. 0.5 g of the biochar sample was added to each flask. The mixtures were incubated for 48 hours. After incubation, the final pH of each suspension was measured. The change in pH (Δ pH) was calculated as: Δ pH = pH(final) – pH(initial) The point of zero charge (pHpzc) is the pH at which Δ pH = 0.

2.3.5 Elemental Analysis

The elemental composition (carbon, hydrogen, and nitrogen, Sulphur) of the biochar samples was determined using a CHN Elemental Analyzer. The oxygen content (%) was calculated by difference using the following equation: O ($\$) = 100 - (C % + H % + N % + Ash %). The atomic ratios of hydrogen to carbon (H/C) and oxygen to carbon (O/C) were subsequently calculated to assess the degree of carbonization and aromaticity of the biochar (Stylianou et al., 2020). For metals analysis, concentrations of K, Fe, Ca, Pb, Cd, and Cr, were quantified using an Atomic Absorption Spectrophotometer (AAS) (PerkinElmer 900H) after digestion.

2.3.6 Determination of Moisture Content

The moisture content of the biochar samples was determined based on mass loss after heating at 105°C for 2 hours following ASTM (2007) procedures. Approximately 1 g of air-dried biochar was weighed into a ceramic crucible and heated in an oven for 2 hours. After heating, the crucible was immediately transferred to a desiccator, allowed to cool for 1 hour, and then reweighed (Aller et al., 2018). The percentage moisture content was calculated using the following equation:

Moisture contents,
$$\% = \frac{[A-B]}{[A]} x100$$
 (3)

Where: A = grams of air-dry sample used, and B = grams of sample after drying at 105° C.

2.3.7. Determination of Volatile Matter

The volatile matter content was determined by heating 1 g of each biochar sample in a preheated muffle furnace at 950°C for 10 minutes in covered crucibles (ASTM, 2007). After heating, the crucibles were cooled in a desiccator for 60 minutes and then weighed. The percentage volatile matter (VM) was calculated using the following equation (4) (Aller et al., 2018):

Volatile matter,
$$\% = \frac{[B-C]}{[B]} x 100$$
 (4)

Where: $C = \text{grams of sample after drying at } 950^{\circ}\text{C}$.

2.3.8 Determination of Ash Content

To determine ash content, 1 g of each biochar sample was placed in a crucible covered with a lid and heated in a muffle furnace at 750°C for 6 hours (ASTM, 2007). The crucibles were cooled in a desiccator for 1 hour and reweighed. Heating was repeated until the difference in weight was less than 0.0005 g in a subsequent 1-hour heating period. The percentage ash content was calculated using the following equation (5) (Aller *et al.*, 2018):

$$qe = \frac{Ci - Ce}{M}xV \tag{5}$$

2.3.9. Specific Surface Area and Cation Exchange Capacity

The specific surface area (SSA) was determined using the Brunauer–Emmett–Teller (BET) method (ASAP 2020 analyzer).

2.3.10. Surface Morphology and Functional Groups

The surface morphology of the biochar samples was examined using scanning electron microscopy (SEM). Functional groups were identified using Fourier-transform infrared spectroscopy (FTIR) in the

range of 400–4000 cm⁻¹. X-ray diffraction (XRD) analysis was performed to determine the crystalline or amorphous nature of the biochars using Cu Kα radiation at 40 kV and 40 mA.

2.1.Batch Adsorption Experiments

Batch adsorption experiments using millet straw generate biochar was performed in 100 cm³ glass conical flasks containing 40 cm³ of Pb(II) solution. The dosage of the biochar samples was 0.3 g. The mixtures were shaken in a temperature oscillator (Bio-shaker BR-23FH) at a constant temperature of 35.5 °C and 120 rpm for 120 min to achieve adsorption equilibrium. The supernatant liquid of the Pb(II) was analyzed with using atomic absorption spectrophotometry AAS (Perkin Elmer 900H).

To explore the kinetics of the adsorption process, batch adsorption experiments was also conducted. The concentrations of Pb(II) solution was selected as 40 cm³ of 150 mg/L was added to 0.3 g of all the adsorbents and then the mixtures were shaken in a temperature oscillator at 35.5 °C and 120 rpm. The samples were taken at predetermined time intervals (5 10, 15, 30, 60, 90, and 120 min) to measure the kinetics. The replicate tests of samples were carried out three times. The Pseudo-first-order equation (7), Pseudo-second-order equation (8), and Elovich model equation. (9), respectively, were used to fit the adsorption isotherms.

The sorption isotherm studies were described as follows. The concentrations of biochar samples were 30, 50, 100, 150 and 200 mg/L. A total 0.3 g of biochar samples each was added to 40 cm³ polluted water samples, and then the mixtures were shaken in a temperature oscillator at 35.5 °C and 120 rpm to adsorption equilibrium. The calculation of equilibrium adsorption capacity (qe, mg/g) at each initial concentration. Then, the isotherm data obtained were fitted using three isotherm models (Langmuir model, Freundlich model, and Temkin model) as given in equations (10-12):

Batch experiments were performed to investigate the effect of biochar dosage and pH. Conical flasks were separately filled with 40 cm³ Pb(II) solution and biochar were kept in an oscillator at 35.5 °C and 120 rpm for 120 min to equilibrium. The adsorption was tested under different biochar dosage from 0.3 to 1,1 g. The initial pH was adjusted to 2, 4, 6, 8 and 10 by 0.1 M NaOH and 0,1M HCl solutions to investigate the effect of original solution pH. The amount of adsorbed on different biochar samples and the removal rate was calculated by Equations (5) and (6) (Qiao *et al.*, 2018):

$$qe = \frac{Ci - Ce}{M}xV \tag{5}$$

$$\%R = \frac{Ci - Ce}{Ci} \times 100$$

Where Ci and Ce are the initial concentration and adsorption equilibrium concentration of Pb^{2+} , respectively (mg·L-1), V is solution volume (L), and m is the mass of BCM (g). The removal rate of the

heavy metal (R%):

$$ln(qe-qt) = ln qe - k1t$$
(7)

$$\frac{t}{qe} = \frac{1}{k_2 q e^2} = \frac{t}{qe} \tag{8}$$

$$qt = \frac{1}{\beta}\ln(\alpha\beta) + \frac{1}{\beta}\ln t \tag{9}$$

Where qt (mg g-1) is the adsorption capacity at time t (min), and k_1 (min-1) and k_2 (g mg-1 min-1) are the rate constants for pseudo-first-order and pseudo-second-order adsorption, respectively (Wu *et al.*, 2019). It is postulated that the Elovich constants α and β , represent the initial adsorption rate (g mg-1 min-2) and the desorption constant (mg g-1 min-1), respectively (Ghasemi et al., 2013).

$$\frac{Ce}{qe} = \frac{Ce}{qm} + \frac{1}{KLqm} \qquad \text{(Langmuir isotherm)} \tag{10}$$

$$RL = \frac{1}{1 + CiKL}$$

$$\log qe = \log KF + \frac{1}{n}\log Ce \text{ (Freundlich isotherm)}$$
 (11)

$$qe = \frac{RT}{h} \ln Ce + \frac{RT}{h} \ln KT \text{ (Temkin isotherm)}$$
 (12)

where qmax (mg g-1) is the maximum adsorption capacity of the biochar, qe (mg g-1) is the equilibrium adsorption capacity, KL (L mg-1) is the Langmuir constant, and KF (mg g-1) (mg L-1) 1/n and 1/n are the Freundlich constants, KT is the Temkin constant (J mol-1), b is the Temkin isotherm equilibrium binding constant (L g-1), R is the gas constant (8.3145 J mol-1 K-1), and T is the absolute temperature at 298 K.

2.1.1. Adsorption Thermodynamics

The thermodynamic study was done so as to determine the (enthalpy change) heat content (ΔH); entropy change (degree of randomness, ΔS), possibility, and spontaneity (Gibbs free energy change, ΔG) in adsorption process. Thermodynamic parameters are required to conclude whether the process is spontaneous or not. Gibb's free energy change, $\Delta G0$, is an indication of the spontaneity of a chemical reaction and therefore is an important criterion for spontaneity. Both enthalpy (ΔH^0) and entropy (ΔS^0) factors must be considered to determine Gibb's free energy of the process (Hanbali et al., 2020)

Thermodynamic parameters for the adsorption of Pb(II) were calculated using the Equation (13) and Van't Hoff equation (14).

$$\Delta G^{O} = -RT \ln K \tag{13}$$

$$\ln K = \frac{\Delta S^0}{R} - \frac{\Delta H^0}{RT} \tag{14}$$

The K value can be obtained from the linearized form of Langmuir equation. The values of ΔG^0 . A Van't Hoff's linear plot of lnK against 1/T was portrayed.

3. Results and Discussion

3.1.1. Fundamental Properties

Table 1 shows results of selected properties of millet straw biochar at four different temperatures (300-600 °C). When the pyrolysis temperature increased from 300 to 600 °C, the biochar yield decreased significantly (p < 0.05) from 48.33 to 28.58%. The significant decline in the biochar yield may be attributed to lost in mass, principally due to loss in moisture and hydrated water, and decomposition and transformation of complex organic compounds into vapor mixed with gases such as water vapor, CO₂, CO, H₂, CH₄, and heavier hydrocarbons (J. Zhang et al., 2014). These results align with previous findings, such as those reported by who observed similar trends in wheat straw biochar yields.

In contrast, the ash content increased from 8.23±0.006 to 18.66±0.006 % as the pyrolysis temperature increased, consistent with trends observed in previous studies Ren (2014). The increase in ash content is mainly due to the concentration of inorganic mineral residues following the volatilization of organic materials. The pH of the biochar samples increased from slightly alkaline 7.45±0.01 at BCM300 to more alkaline values at BCM600 10.39±0.05. This trend is attributed to the thermal decomposition of acidic functional groups and the enrichment of alkali-containing minerals at higher temperatures (Hu et al., 2022). The electrical conductivity (EC), **Table 1** which reflects the soluble salt content in the biochar, significantly increased from 4.50±0.12 to 16.12±0.02 mS/cm as the pyrolysis temperature rose. This increase is likely related to the higher ash content and increased release of soluble ions at elevated temperatures (Askeland *et al.*, 2019).

Conversely, the cation exchange capacity (CEC) decreased from 75.60±0.21 cmol/kg to 28.60±0.02 cmol/kg as the pyrolysis temperature increased. This decline is associated with the loss of oxygen-containing functional groups, such as carboxyl and phenolic groups, which contribute to cation exchange sites (Claoston *et al.*, 2014). The point of zero charge (pHpzc) also increased with pyrolysis temperature from 7.10 to 9.50, indicating that higher temperatures result in biochars with more basic surfaces due to the thermal decomposition of acidic surface groups (Di *et al.*, 2025). When the solution pH is lower than the pHpzc, the biochar surface is positively charged, favoring the adsorption of anions. When the solution pH is higher than the pHpzc, the surface is negatively charged, promoting cation adsorption (Le *et al.*, 2019). The specific surface area (SSA) **Table 1** of the biochar increased significantly with

temperature, from 281.99 m²/g at 300 °C to 404.28 m²/g at 600 °C. This enhancement is attributed to the volatilization of pore-blocking substances, resulting in the development of more porous structures (Gaffar *et al.*, 2021).

Table 1: Fundamental properties of millet straw biochar

Biochar	BCM300	BCM400	BCM500	BCM600
Yield (%)	48.33 ± 0.020 a	40.67 ± 0.520 b	34.45± 0.514c	28.58± 0.020d
pH	7.45±0.01c	9.57±0.01b	10.48±0.03a	$10.39 \pm 0.05a$
EC (mS/cm)	4.50±0.12d	7.43±0.03c	13.87±0.01b	16.12±0.02a
CEC (cmol/kg)	$28.60 \pm 0.02a$	64.40±0.02b	71.11±0.02c	75.60±0.21d
Ash content (%)	$8.23 \pm 0.006a$	10.55±0.006b	15.23±0.006c	18.66±0.006d
SSA (m2/g)	281.992	334.666	347.909	404.284
pHpzc	7.10	9.10	9.30	9.50

Each value represents the mean of three replicates (n=3), \pm standard deviation. Small letters following the numerical values denote significant differences between each row data (p < 0.05). However, means that do not share a letter are significantly different.

3.2. Elemental Composition

The elemental analysis Table 2 showed that carbon content increased with pyrolysis temperature, while hydrogen and oxygen contents decreased, indicating the carbonization and dehydration of the biomass (Zhenyu et al., 2013). The decreasing H/C and O/C ratios suggest a higher degree of aromaticity and thermal stability at elevated temperatures. Additionally, the C/N ratio increased with temperature, indicating nitrogen loss and structural transformation (Shi *et al.*, 2019). The concentrations of potassium (K), calcium (Ca), and iron (Fe) increased with temperature, likely due to mineral concentration in the biochar ash. The levels of heavy metals such as Pb and Cr were not detected in the biochar, confirming the safety of the produced adsorbent (Yanga *et al.*, 2013). Each value represents the mean of three replicates (n=3), \pm standard deviation. Small letters following the numerical values denote significant differences between each row data (p < 0.05).

3.2.1. Functional groups Analysis

The FTIR spectra **Figure 1** of the biochars revealed key functional groups contributing to Pb(II) adsorption. Peaks observed at 2922 cm⁻¹ and 3755 cm⁻¹ were attributed to methyl C−H stretching and phenolic −OH groups, respectively Peaks between 2113–2117 cm⁻¹ correspond to terminal alkyne C≡C

stretching (Qiao et al., 2020). Bands between 1580–1509 cm⁻¹ indicated aromatic C=C stretches from lignin structures (Zahedifar et al., 2021). Peaks at 872 cm⁻¹ and 779 cm⁻¹ were associated with Si–O–Si stretching vibrations (Di et al., 2025), reflecting the silicon-rich nature of millet straw.

Table 2: El	emental anal	vsis of th	he three o	different	biochars	Biochar
I abic 2. Li	CIIICIItai aiiai	vois of u	ne unice i	unitation	orochars.	Diochai

Biochar	BCM300	BCM400	BCM500	BCM600
C (%)	57.33±0.006d	61.67±0.006c	69.43±0.006b	74.24±0.006a
H (%)	4.63±0.006a	3.57 ± 0.006 b	2.48±0.006c	$0.97 \pm 0.006 d$
O (%)	28.34±0.0061	21.18±0.01b	12.06±0.001c	5.39±0.001d
N (%)	1.46±0.006a	$1.03 \pm 0.02b$	$0.76 \pm 0.06c$	$0.46 \pm 0.02 d$
H/C	0.962	0.689	0.426	0.156
O/C	0.371	0.269	0.130	0.055
C/N	0.022	0.014	0.009	0.005
K(mg/kg)	57.55±0.202c	57.66±1.095c	81.5±1.252b	$131.1 \pm 0.54a$
Ca(mg/kg)	17.67±0.017d	19.02±0.018c	$25 \pm 0.050 b$	30.66±0.073a
Fe(mg/kg)	$0.388 \pm 0.0140b$	0.49 ± 0.0071 b	0.523±0.0094b	$0.523 \pm 0.0094b$
Pd(mg/kg)	ND	ND	ND	ND
Cd(mg/kg)	$0.01\pm0.0013a$	$0.01 \pm 0.0005a$	0.007±0.0006a	$0.009\pm0.001a$
Cr(mg/kg)	ND	ND	ND	ND

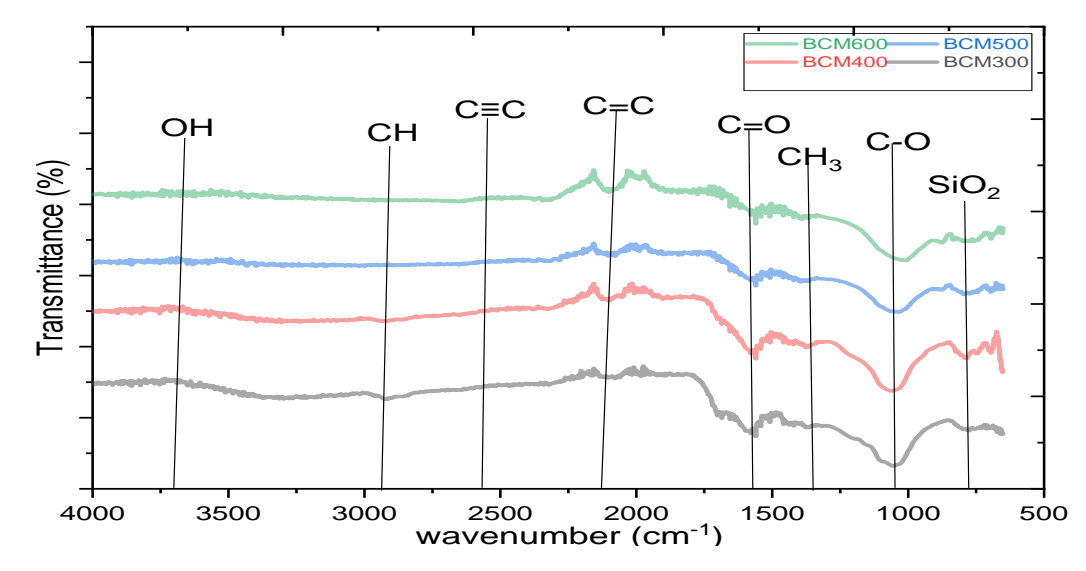


Figure 1: FT-IR Spectrum of millet straw biochars produced at different pyrolysis temperatures.

3.2.2. Scanning Electron Microscope (SEM)

SEM images Figure 2 showed that biochar produced at lower temperatures (300 °C) had smoother surfaces with less-developed pores, while biochar produced at higher temperatures (600 °C) exhibited

rougher, highly porous structures. The increase in porosity with pyrolysis temperature is consistent with enhanced devolatilization and pore development (Zhao *et al.*, 2023).

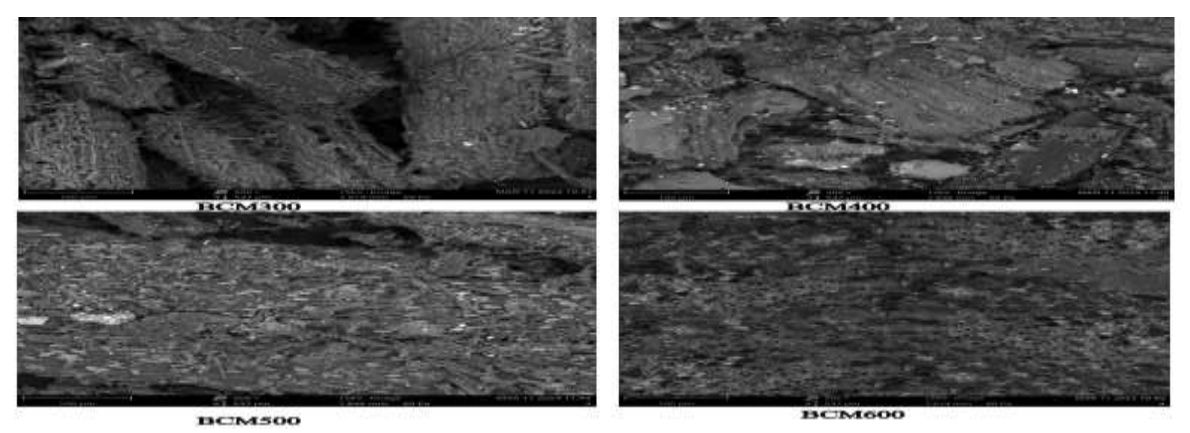


Figure 2: SEM Images of millet straw biochar pyrolyzed at 300, 400, 500, and 600°C at 500X magnification.

3.3.XRD Analysis

XRD patterns **Figure 3** indicated that the biochars were predominantly amorphous with broad, low-intensity peaks. The presence of SiO₂ was confirmed by peaks around $2\theta = 21.37^{\circ}$, while peaks at 43.2° were attributed to graphene-like structures (Li, 2020). Minor peaks at 50.7° and 81.2° suggested the presence of calcite (Wang *et al.*, 2025). The overall amorphous structure is favorable for adsorption due to increased surface activity (Ampofo *et al.*, 2021).

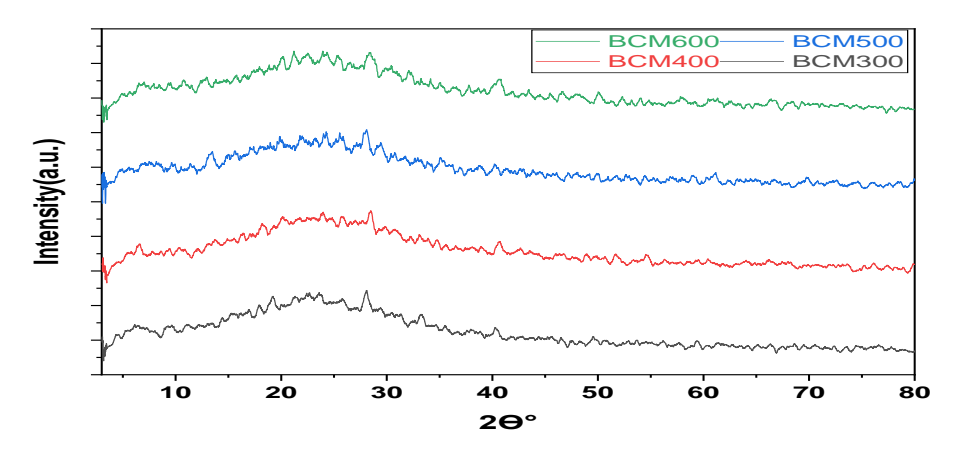


Figure 3: XRD spectra of millet straw biochar at four different temperatures

3.4. Adsorption experiments

Effect of Biochar Dosage and Initial pH

As shown in **Figures 4a and 4b**, Pb(II) adsorption capacity and removal efficiency increased with solution pH from 2 to 6. At low pH, excess H⁺ ions compete with Pb²⁺ for adsorption sites (Tho *et al.*, 2021). As the pH approaches neutral, H⁺ competition decreases and electrostatic attraction between Pb²⁺ ions and negatively charged biochar surfaces increases (Singh *et al.*, 2023). Above pH 6, Pb(II) ions

may hydrolyze to form insoluble Pb(OH)₂, reducing adsorption efficiency (K. Zhang *et al.*, 2018). Figures 5a and 5b showed that increasing biochar dosage reduced the adsorption capacity per unit mass but increased the overall removal efficiency. At higher dosages, the aggregation of biochar particles can lead to site overlap and reduced accessibility (Ramachandran *et al.*, 2011). However, the greater number of available active sites enhances total Pb(II) removal efficiency (Pap *et al.*, 2018).

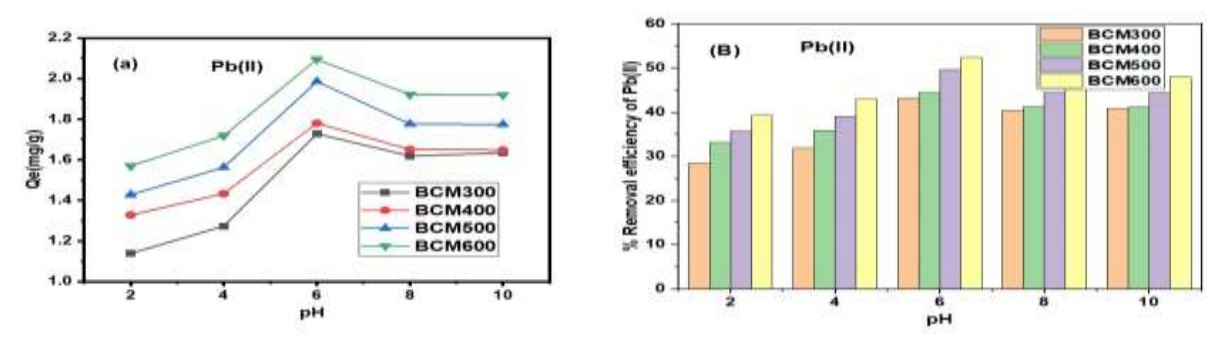


Figure 4: Effect of pH on the adsorption of Pb(II) ions (a) adsorption capacity (b) removal efficiency on millet straw biochar prepared from four different temperatures.

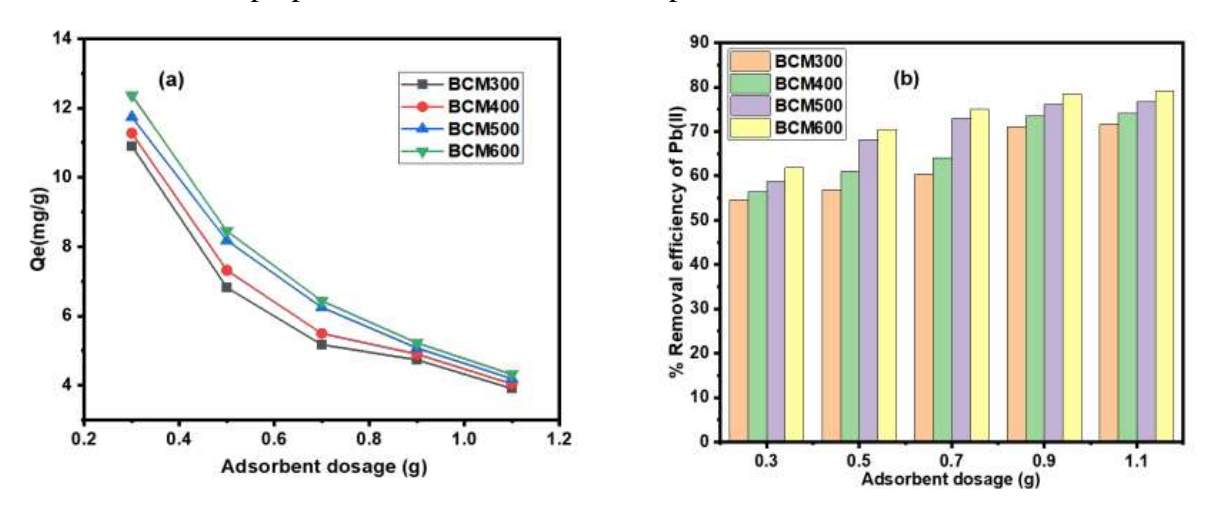


Figure 5: Effect of adsorbent dose on the adsorption on the adsorption of Pb(II) ions (a) adsorption capacity (b) removal efficiency on millet straw biochar prepared at four different temperatures.

3.4.1. Adsorption Isotherms

Adsorption isotherm describe the equilibrium relationship between adsorbent and adsorbate (Qiao et al., 2018). The adsorption isotherms of Pb(II) onto BCM-biochar at 35.5 °C are presented in **Figure 6.** According to the slope obtained by plotting 1/qe versus 1/ce and the intercept from lnqe versus lnCe, the parameters of the Langmuir, Freundlich and Temkin models were computed and presented in **Table 3**. Isotherm fitting showed that the Langmuir model best described Pb(II) adsorption onto biochar (R² = 0.94–0.97), indicating monolayer adsorption on a homogenous surface (K. Singh *et al.*, 2023). The Freundlich and Temkin models provided acceptable but less accurately fits, suggesting that some degree

of multilayer adsorption and adsorbate-adsorbate interactions may occur (Huang *et al.*, 2022). The separation factor (R_L) values (0.066–0.094) confirmed favorable adsorption conditions (Chen *et al.*, 2023).

Table 3: Regression parameters of Langmuir, Freundlich and Temkin models for adsorption of Pb²⁺ by biochars.

Metal	Biochar Lan		Freundlich Isotherm			Temkin Isotherm				
		Qmax	KL	R²	KF	1/n	R ²	b _T (J mol-1)	K_{T}	R ²
	BCM300	9.76	0.089	0.94	2.19	0.292	0.79	1.98	0.749	0.87
Pb (II)	BCM400	10.49	0.066	0.97	2.27	0.299	0.84	2.13	0.72	0.92
	BCM500	11.18	0.094	0.96	2.37	0.303	0.84	2.29	0.69	0.92
	BCM600	11.82	0.090	0.94	2.59	0.296	0.81	2.39	0.74	0.89

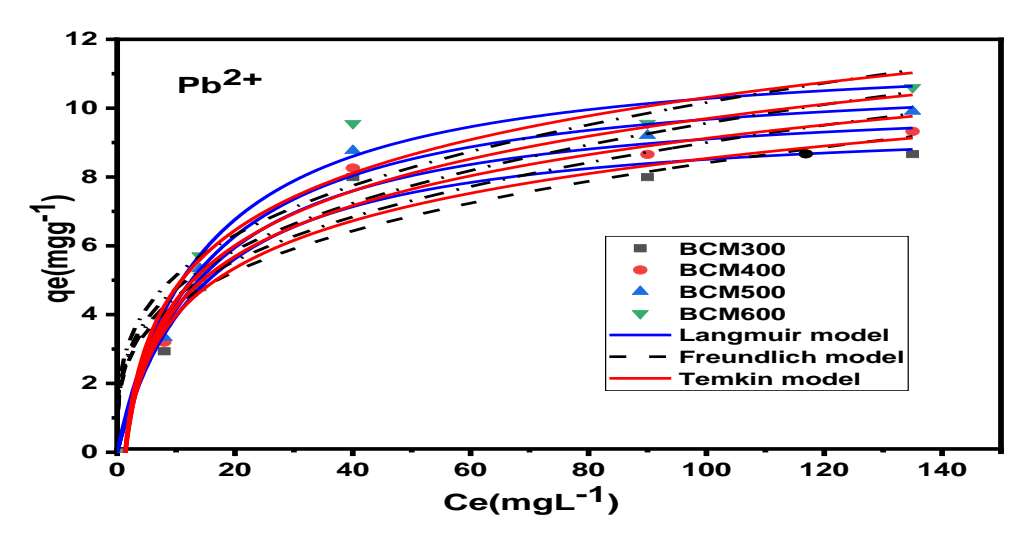


Figure 6: Adsorption isotherm of Pb (II) by BCM300, BCM400, BCM500, and BCM600 described by Langmuir, Freundlich and Temkin models.

3.4.2. Adsorption Kinetics

Figure 7 illustrates the amounts of Pb²⁺ ion adsorbed by BCM300, BCM400, BCM500 and BCM600 as a function of adsorption time (0-120min). The effect of time on the adsorption of Pb(II) onto biochar is an important factor in understanding the adsorption kinetics and optimizing treatment processes (Chen *et al.*, 2023). The adsorption of Pb(II) onto biochar is time dependent, with rapid removal occurring within the first 30 minutes due to the availability of active surface adsorption, followed by a slower phase dominated by intraparticle diffusion. Equilibrium is typically reached between 90 and 120 minutes, after which further adsorption was minimal (Singh *et al.*, 2023).

The pseudo-first-order, pseudo-second-order and Elovich models were used to evaluate the adsorption of Pb(II) in this study (Aaddouz *et al.*, 2023). The adsorption of Pb onto biochar is best described by the

pseudo-second-order model, as indicated by the highest values (0.995–0.999). This suggests that chemisorption is the primary mechanism, supported by strong interactions between Pb ions and active sites on the biochar. The pseudo-first-order and Elovich models provide less accurate fits but may offer supplementary insights into specific aspects of the adsorption process (Wu *et al.*, 2019). Furthermore, the equilibrium adsorption capacities (qe exp.) **Table 4**, shows that Pseudo-second order model is the most accurate for describing the Pb(II) adsorption onto biochar, as its (qe cal.) values are nearly identical to (qe exp.). This further corroborates that the adsorption mechanism is dominated by chemisorption, involving strong interactions between Pb (II) ions and the biochar surface (XChen *et al.*, 2011).

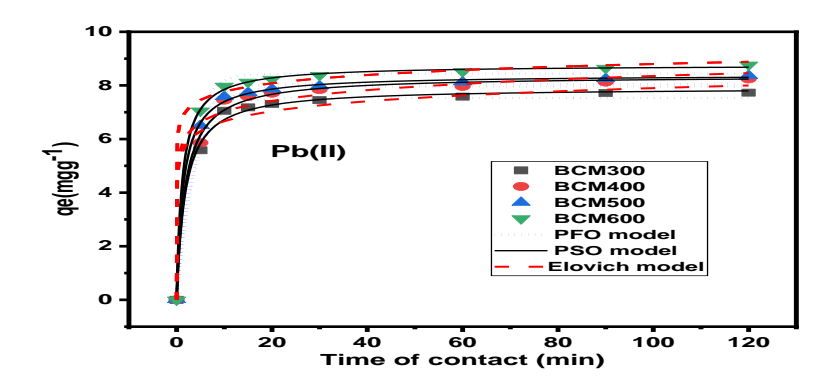


Figure 7: Kinetic adsorption of Pb (II) by BCM300, BCM400, BCM500, and BCM600 described by Pseudo first order, Pseudo second order and Elovich models

Table 4. Regression parameters of Pseudo-first-order, Pseudo-second-order and Elovich models for adsorption of Pb²⁺ by BCM prepared from four different temperatures

Meta	al Bio	char	P	seudo fi	rst order		Pseudo	second	order	Elovich mo	del	
		Qe	Qe			Qe	Qe					
	Biochar	exp	cal.	k1	R ²	exp	cal.	k2	R ²	a	b	R ²
	BCM300	7.73	7.54	0.266	0.996	7.73	7.91	0.071	0.996	13638.69	1.867	0.98
Pb	BCM400	8.24	7.96	0.264	0.995	8.24	8.37	0.066	0.995	10978.65	1.731	0.98
	BCM500	8.36	8.05	0.317	0.995	8.36	8.39	0.088	0.999	222617.59	2.098	0.99
	BCM600	8.77	8.44	0.347	0.994	8.77	8.76	0.097	0.999	1.56E+06	2.235	0.99

3.4.3. Thermodynamics Analysis

Pyrolysis temperature significantly influences the properties of millet straw biochar and its effectiveness in Pb(II) adsorption. Higher pyrolysis temperatures favour an increase in adsorption capacity due enhance structural properties (Fan et al., 2016). Increase in the percentage removal efficiency was attained with an increase in temperature of the system supporting the endothermic process. This is due

to a decrease in the mass transfer resistance and boundary layer thickness of BCM (Dada *et al.*, 2021). (**Table 5**) shows that increase in temperature from 300- 600°C increases the positive ΔH value from ΔH (+12.678 to +23.627kJ mol⁻¹), respectively.

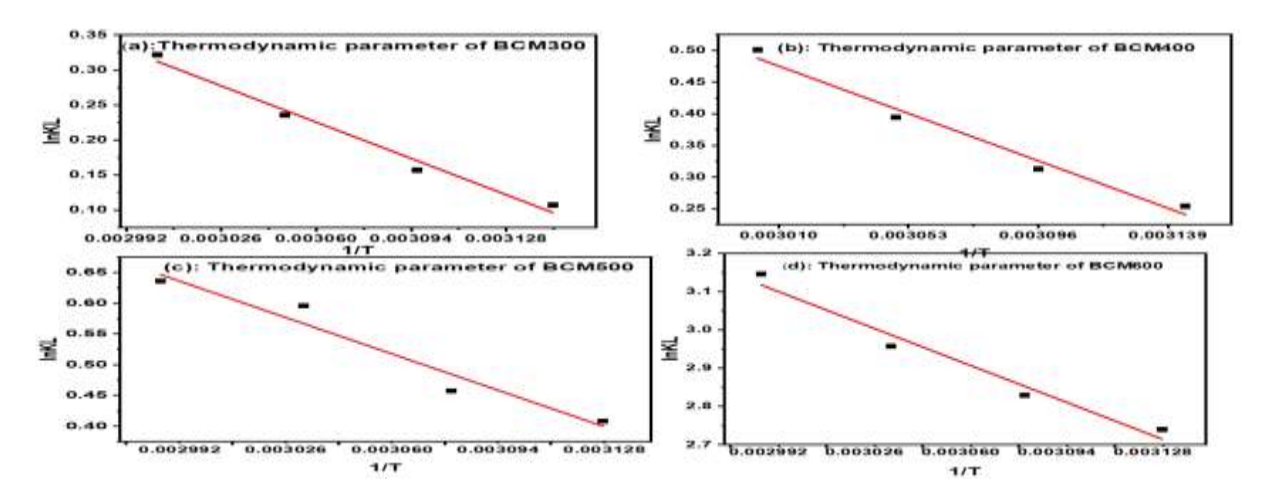


Figure 8. Van't Hoff's plot for the adsorption of Pb (II) onto millet straw biochar prepared at four different temperatures.

Table 5. Thermodynamic parameters for adsorption of Pb(II) onto BCM at four different temperatures

Biochar	Temperature (K)	ΔG^0 (Jmol-1)	ΔH ^o (KJmo-1)	ΔS ⁰ (KJmol-1)	\mathbb{R}^2
BCM300	318	-284.35	+12.678	+40.67	0.98
	323	-422.65			
	328	-643.73			
	333	-890.76			
BCM400	318	-671.48	+14.473	+47.52	0.97
	323	-839.59			
	328	-1075.50			
	333	-1387.75	+14.443	+48.75	0.93
BCM500	318	-1080.21			
	323	-1229.17			
	328	-1624.15			
	333	-1760.81	+23.627	+96.87	0.95
BCM600	318	-7244.25			
	323	-7597.53			
	328	-8064.09			
	333	-8709.16			
-					

Confirming that the adsorption process is endothermic in nature (J. Liu et al., 2022). The positive ΔS values increase from ΔS (+ 40.67 to 96.867Jmol-1 K⁻¹), with respective increase in pyrolysis temperature, which shows an increase in the degree of randomness of the interaction during the adsorption of Pb²⁺ at the solid/liquid interface. The feasibility and spontaneity of the adsorption process are confirmed by the negative values of ΔG (Zhao *et al.*, 2023).

Conclusion

This study investigated the removal of Pb(II) heavy metal in aqueous solutions by millet straw biochar and explored the underlying adsorption mechanism. The biochars were systematically investigated by determining their physicochemical properties and using conventional characterization techniques. Pyrolysis temperature strongly influenced the physical and chemical properties of the biochars produced from millet straw. The temperature at which the biomass was pyrolyzed had a significant effect. The results indicate that biochar produced at 600 °C from millet straw may provide an effective way to enhance heavy metal removal from aqueous solutions. The results of isothermal adsorption experiments showed that the Langmuir equation could better describe the adsorption process well among four biochars for Pb(II), mainly monolayer adsorption. The pseudo-second-order model was more suitable for describing the adsorption process of metal ions by biochar. The adsorption thermodynamic process $\Delta G_{\theta} < 0$, $\Delta H_{\theta} > 0$, $\Delta S > 0$ indicated that adsorption was a spontaneous, endothermic and disordered process.

Acknowledgement

The authors wish to thank the department of Pure and Industrial Chemistry, Bayero University, Kano, Nigeria.

References

- Aaddouz M., Azzaoui K., Akartasse N., Mejdoubi E., Hammouti B., Taleb M., Sabbahi R., Alshahateet S.F. (2023). Removal of Methylene Blue from aqueous solution by adsorption onto hydroxyapatite nanoparticles, *Journal of Molecular Structure*, 1288, 135807, https://doi.org/10.1016/j.molstruc.2023.135807
- Aller, D., Aller, D., Bakshi, S., & Laird, D. A. (2018). Modified method for proximate analysis of biochars. *Journal of Analytical and Applied Pyrolysis*, 124(January 2017), 335–342. https://doi.org/10.1016/j.jaap.2017.01.012
- Alluqmani, S. M., Saedoon, H., Neftel, A., Shwe, K. K., Chaopayao, N., & Yampracha, S. (2019). Effect of Pyrolysis Temperature and Time on Properties of Palm Kernel Shell-Based Biochar Effect of Pyrolysis Temperature and Time on Properties of Palm Kernel Shell-Based Biochar. *IOP Conference Series:*Materials Science and Engineering. https://doi.org/10.1088/1757-899X/548/1/012020
- Ampofo, E., Id, S., Song, Y., Yu, Y., & Zhuang, H. (2021). Biochars derived from bamboo and rice straw for sorption of basic red dyes. *PLose ONE*, 16(7), 1–20. https://doi.org/10.1371/journal.pone.0254637

- Askeland, M., Clarke, B., & Paz-ferreiro, J. (2019). Comparative characterization of biochars produced at three selected pyrolysis temperatures from common woody and herbaceous waste streams. *PeerJ*, 1–20. https://doi.org/10.7717/peerj.6784
- Audu, A., & Idowu, A. (2015). The Effect of the Challawa Industrial Estate on the Physicochemical Properties and Heavy Metal Levels of Portable Water Supply in Kano Metropolis, Nigeria. April, 17–22.
- Chen, Q., Gao, M., Miao, Q., Xiao, L., Li, Z., Qiu, W., & Song, Z. (2023). Characteristics of a Novel Decomposed Corn Straw-Sludge Biochar and Its Mechanism of Removing Cadmium from Water. *ACS OMEGA*, *Ii*. https://doi.org/10.1021/acsomega.3c01196
- Chen, X., Chen, G., Chen, L., Chen, Y., Lehmann, J., Mcbride, M. B., & Hay, A. G. (2011). Adsorption of copper and zinc by biochars produced from pyrolysis of hardwood and corn straw in aqueous solution. *Bioresource Technology*, 102(19), 8877–8884. https://doi.org/10.1016/j.biortech.2011.06.078
- Chen, Y., Lin, Y., Ho, S., Zhou, Y., & Ren, N. (2018). Highly efficient adsorption of dyes by biochar derived from pigments- extracted macroalgae pyrolyzed at di ff erent temperature. *Bioresource Technology*, 259(January), 104–110. https://doi.org/10.1016/j.biortech.2018.02.094
- Claoston, N., Samsuri, A. W., Husni, M. H. A., & Amran, M. S. M. (2014). Effects of pyrolysis temperature on the physicochemical properties of empty fruit bunch and rice husk biochars. *Waste Management and Research*, 32(4), 331–339. https://doi.org/10.1177/0734242X14525822
- Dada, A. O., Adekola, F. A., Odebunmi, E. O., & Ogunlaja, A. S. (2021). Two three parameters isotherm modeling, kinetics with statistical validity, desorption and thermodynamic studies of adsorption of Cu(II) ions onto zerovalent iron nanoparticles. *Scientific Reports*, 1–15. https://doi.org/10.1038/s41598-021-95090-8
- Di, D., Xiao, J., Zhao, B., Chen, Y., Song, Z., & Chen, G. (2025). Immobilization of Cd (II) by phosphorus modified bamboo biochar from solution: mechanistic study from qualitative to quantitative analysis. *Carbon Research*, 4(35). https://doi.org/10.1007/s44246-025-00196-7
- El Hammari L., Latifi S., Saoiabi S., Saoiabi A., Azzaoui K., Hammouti B., Chetouani A., Sabbahi R. (2022), Toxic heavy metals removal from river water using a porous phospho-calcic hydroxyapatite, *Mor. J. Chem.* 10(1), 62-72, https://doi.org/10.48317/IMIST.PRSM/morjchem-v10i1.31752
- Errich A., Azzaoui K., Mejdoubi E., Hammouti B., Abidi N., Akartasse N., Benidire L., EL Hajjaji S., Sabbahi R., Lamhamdi A. (2021), Toxic heavy metals removal using a hydroxyapatite and hydroxyethyl cellulose modified with a new Gum Arabic, *Indonesian Journal of Science & Technology*, 6(1), 41-64
- Fan, S., Tang, J., Wang, Y., Li, H., Zhang, H., Tang, J., Wang, Z., & Li, X. (2016). Biochar prepared from copyrolysis of municipal sewage sludge and tea waste for the adsorption of methylene blue from aqueous solutions: Kinetics, isotherm, thermodynamic and mechanism. *Journal of Molecular Liquids*, 220, 432–441. https://doi.org/10.1016/j.molliq.2016.04.107
- Feng, C., Li, J., Jiang, W., Liu, J., & Xue, Q. (2023). Geo environmental and mechanical behaviors of As (V) and Cd (II) co contaminated soils stabilized by goethite nanoparticles modified biochar. *Biochar*, 553. https://doi.org/10.1007/s42773-023-00253-7
- Fouda-Mbanga B.G., Velempini T., Pillay K., Tywabi-Ngeva Z. (2024). Heavy metals removals from wastewater and reuse of the metal loaded adsorbents in various applications: A review, *Hybrid Advances*, 6, 100193, ISSN 2773-207X, https://doi.org/10.1016/j.hybadv.2024.100193
- Gaffar, S., Dattamudi, S., Baboukani, A. R., Chanda, S., Novak, J. M., Watts, D. W., Wang, C., & Jayachandran, K. (2021). Physiochemical Characterization of Biochars from Six Feedstocks and Their Effects on the Sorption of Atrazine in an Organic Soil. *Agronomy*, 1–18.
- Gang Yanga, Zhanghong Wangb, Q. X., , Fei Shen, C. S., & Yanzong Zhang, J. W. (2013). Physicochemical

- properties of biochar derived from vermicompost as affected by pyrolysis temperature and potential environmental amendment as an adsorbent. *Royal Society of Chemistry*.
- Ghasemi, M., Naushad, M., Ghasemi, N., & Khosravi-fard, Y. (2013). Adsorption of Pb (II) from aqueous solution using new adsorbents prepared from agricultural waste: Adsorption isotherm and kinetic studies. *Journal of Industrial and Engineering Chemistry*. https://doi.org/10.1016/j.jiec.2013.09.050
- Hanbali, G., Jodeh, S., Hamed, O., Bol, R., & Khalaf, B. (2020). Enhanced Ibuprofen Adsorption and Desorption on Synthesized Functionalized Magnetic Multiwall Carbon Nanotubes from Aqueous Solution. *Materials*, 1–22.
- Kankou M. S.'A., N'diaye A. D., Hammouti B., Kaya S. and Fekhaoui M. (2021) Ultrasound-assisted adsorption of Methyl Parathion using commercial Granular Activated Carbon from aqueous solution, *Mor. J. Chem.* 9(4), 832-842 768)
- Hu, X., Zhang, R., Xia, B., Ying, R., Hu, Z., Tao, X., & Yu, H. (2022). Effect of Pyrolysis Temperature on Removal Efficiency and Mechanisms of Hg (II), Cd (II), and Pb (II) by Maize Straw Biochar. *Sustainability*, 1–16.
- Huang, A., Bai, W., Yang, S., Wang, Z., Wu, N., Zhang, Y., Ji, N., & Li, D. (2022). Adsorption Characteristics of Chitosan-Modified Bamboo Biochar in Cd (II) Contaminated Water. *Hindawi Journal of Chemistry*, 1–10.
- Le, D. T., Phuong, T., Le, T., Do, H. T., Vo, H. T., Pham, N. T., Nguyen, T. T., Cao, H. T., Nguyen, P. T., Mai, T., Dinh, T., Le, H. V., & Tran, D. L. (2019). Fabrication of Porous Hydroxyapatite Granules as an Effective Adsorbent for the Removal of Aqueous Pb (II) Ions. *Hindawi Journal of Chemistry*, 2019, 1–10.
- Li, Y. (2020). Adsorption behaviors on trace Pb 2 b from water of biochar adsorbents from konjac starch. *Adsortion Science and Technology*, *38*(9–10), 344–356. https://doi.org/10.1177/0263617420948699
- Liu, H., Xu, F., Xie, Y., Wang, C., Zhang, A., Li, L., & Xu, H. (2018). Effect of modi fi ed coconut shell biochar on availability of heavy metals and biochemical characteristics of soil in multiple heavy metals contaminated soil. *Science of the Total Environment*, 645, 702–709. https://doi.org/10.1016/j.scitotenv.2018.07.115
- Liu, J., Wang, H., Ma, N., Zhou, B., Chen, H., & Yuan, R. (2022). Optimization of the raw materials of biochars for the adsorption of heavy metal ions from aqueous solution. *Water Science & Technology*, 00(0), 1–13. https://doi.org/10.2166/wst.2022.158
- Loc, N. X., Thanh, T. D., Thi, D., & Phuong, M. (2023). Physicochemical properties of biochar produced from biodegradable do- mestic solid waste and sugarcane bagasse. *International Journal of Recycling of Organic Waste in Agriculture*, 12, 395–407. https://doi.org/10.30486/IJROWA.2022.1954704.1429
- Machida, M., Kikuchi, Y., Aikawa, M., & Tatsumoto, H. (2019). Kinetics of adsorption and desorption of Pb(II) in aqueous solution on activated carbon by two-site adsorption model. *Collloid and Surfaces*, *July*. https://doi.org/10.1016/j.colsurfa.2004.04.046
- Mahmoud, E. R. I., Aly, H. M., Hassan, N. A., Aljabri, A., Khan, A. L., & El-labban, H. F. (2024). Utilizing Date Palm Leaf Biochar for Simultaneous Adsorption of Pb (II) and Iodine from Aqueous Solutions Utilizing Date Palm Leaf Biochar for Simultaneous Adsorption. *Processes*, *Ii*.
- Meftah, S., Meftah, K., Drissi, M. et al. (2025). Heavy metal polluted water: Effects and sustainable treatment solutions using bio-adsorbents aligned with the SDGs. *Discov Sustain* 6, 137, https://doi.org/10.1007/s43621-025-00895-6
- Osman, A. I., Fawzy, S., Farghali, M., El, M., Ahmed, A., & Rooney, D. W. (2022). Biochar for agronomy, animal farming, anaerobic digestion, composting, water treatment, soil remediation, construction, energy storage, and carbon sequestration: a review. In *Environmental Chemistry Letters* (Vol. 20, Issue 4). Springer International Publishing. https://doi.org/10.1007/s10311-022-01424-x

- Pap, S., Bezanovic, V., Radonic, J., Babic, A., Saric, S., Adamovic, D., & Turk, M. (2018). Synthesis of highly-ef fi cient functionalized biochars from fruit industry waste biomass for the removal of chromium and lead. *Journal of Molecular Liquids*, 268, 315–325. https://doi.org/10.1016/j.molliq.2018.07.072
- Pet, I., Sanad, M.N., Farouz, M. et al. Review: Recent Developments in the Implementation of Activated Carbon as Heavy Metal Removal Management. Water Conserv Sci Eng 9, 62 (2024). https://doi.org/10.1007/s41101-024-00287-3
- Qiao, K., Tian, W., Bai, J., Dong, J., Zhao, J., Gong, X., & Liu, S. (2018). Preparation of biochar from Enteromorpha prolifera and its use for the removal of polycyclic aromatic hydrocarbons (PAHs) from aqueous solution. *Ecotoxicology and Environmental Safety*, 149(November 2017), 80–87. https://doi.org/10.1016/j.ecoenv.2017.11.027
- Qiao, K., Tian, W., Bai, J., Zhao, J., & Du, Z. (2020). Synthesis of floatable magnetic iron / biochar beads for the removal of chromium from aqueous solutions. *Environmental Technology & Innovation*, 19, 100907. https://doi.org/10.1016/j.eti.2020.100907
- Ramachandran, P., Vairamuthu, R., & Ponnusamy, S. (2011). Adsorption isotherms, kinetics, thermodynamics and desorption studies of reactive orange16 on activated carbon derived from Ananas comosus (L.) Carbon. *Journal of Engineering and Applied Sciences*, 6(11), 15–26.
- Ren, L. (2014). Influence of pyrolysis temperature on characteristics and heavy metal adsorptive performance of biochar derived from municipal sewage sludge. *BIORESOURCE TECHNOLOGY*. https://doi.org/10.1016/j.biortech.2014.04.048
- Shi, J., Fan, X., Tsang, D. C. W., Wang, F., Shen, Z., Hou, D., & Alessi, D. S. (2019). Removal of lead by rice husk biochars produced at different temperatures and implications for their environmental utilizations. *Chemosphere*, 235, 825–831. https://doi.org/10.1016/j.chemosphere.2019.06.237
- Singh, Amit Kumar Dimitrios, G., Michael, A., Triantafyllidis, K. S., & Nair, V. (2023). Composites of Lignin-Based Biochar with BiOCl for Photocatalytic Water Treatment: RSM Studies for Process Optimization. *Nanomaterials*.
- Singh, K., Azad, S. K., Dave, H., Prasad, B., Maurya, D. M., Kumari, M., Dubey, D., Rai, A. K., Sillanpää, M., Sah, M. P., & Prasad, K. S. (2023). Effective removal of Cr (VI) ions from the aqueous solution by agrowaste based biochar: an exploration of batch and column studies. *Biomass Conversion and Biorefinery*, *July*. https://doi.org/10.1007/s13399-023-04268-9
- Singh, V., Pant, N., Sharma, R. K., Padalia, D., & Rawat, P. S. (2023). Adsorption Studies of Pb(II) and Cd(II) Heavy Metal Ions from Aqueous Solutions Using a Magnetic Biochar Composite Material. *Separation Science and Technology*, 10(389), 1–17.
- Stylianou, M., Christou, A., Dalias, P., Polycarpou, P., Michael, C., *et al.* (2020). Physicochemical and structural characterization of biochar derived from the pyrolysis of biosolids, cattle manure and spent coffee grounds. *Journal of the Energy Institute*, 1–44. https://doi.org/10.1016/j.joei.2020.05.002
- Tho, P. T., Van, H. T., Nguyen, H., Hoang, K., & Ha, N. (2021). Enhanced simultaneous adsorption of As (III), Cd (II), Pb (II) and Cr (VI) ions from aqueous solution using cassava root husk-derived biochar loaded with ZnO nanoparticles. *Royal Society of Chemistry*, 11, 18881–18897. https://doi.org/10.1039/d1ra01599k
- Wang, W., Wei, P., Wang, C., Liang, P., Tao, F., Yang, S., & Dou, W. (2025). Honeycomb structured biochar from waste pomelo peel for synergistic adsorptive and photocatalytic removal of Cr(VI). *Carbon Research*, 410, 1–19. https://doi.org/10.1007/s44246-024-00174-5
- Wu, Xian, Y., He, Z., Zhang, Q., Wu, J., Yang, G., & Zhang, X. (2019). Adsorption characteristics of Pb (II) using biochar derived from spent mushroom substrate. *Scientific Reports*, *Ii*, 1–11. https://doi.org/10.1038/s41598-019-52554-2

- Yuan, J., Wang, C., Tang, Z., Chu, T., Zheng, C., Han, Q., Chen, H., & Tan, Y. (2024). Biochar derived from traditional Chinese medicine residues: An efficient adsorbent for heavy metal Pb (II). *Arabian Journal of Chemistry*, 17(3), 105606. https://doi.org/10.1016/j.arabjc.2024.105606
- Zahedifar, M., Seyedi, N., Shafiei, S., & Basij, M. (2021). Surface-modified magnetic biochar: Highly efficient adsorbents for removal of Pb (II) and Cd (II). *Materials Chemistry and Physics*, 271(May), 124860. https://doi.org/10.1016/j.matchemphys.2021.124860
- Zhang, J., Liu, R. (2014). Effects of pyrolysis temperature and heating time on biochar obtained from the pyrolysis of straw and lignosulfonate. *Bioresource Technology*. https://doi.org/10.1016/j.biortech.2014.11.011
- Zhang, K., Sun, P., Faye, M. C. A. S., & Zhang, Y. (2018). Characterization of biochar derived from rice husks and its potential in chlorobenzene degradation. *Carbon*, 1–36. https://doi.org/10.1016/j.carbon.2018.01.036
- Zhang, N., Reguyal, F., Praneeth, S., & Sarmah, A. K. (2023). A novel green synthesized magnetic biochar from white tea residue for the removal of Pb (II) and Cd (II) from aqueous solution: Regeneration and sorption mechanism. *Environmental Pollution*, 330(May), 121806. https://doi.org/10.1016/j.envpol.2023.121806
- Zhao, H., Liu, J., Li, J., Shi, E., Wang, C., Yang, J., Zhang, Z., Wang, S., Zhao, H., Liu, J., Wang, X., Li, J., Shi, E., Wang, C., Yang, J., & Zhang, Z. (2023). A study on and adsorption mechanism of ammonium nitrogen by modified corn straw biochar. *Royal Society Open Science*, 10(221535), 1–12.
- Zhenyu, Zheng, H., Luo, Y., Deng, X., Herbert, S., & Xing, B. (2013). Characterization and influence of biochars on nitrous oxide emission from agricultural soil. *Environmental Pollution*, 174, 289–296. https://doi.org/10.1016/j.envpol.2012.12.003
- Zhou, R., Zhang, M., Li, J., & Zhao, W. (2020). Optimization of preparation conditions for biochar derived from water hyacinth by using response surface methodology (RSM) and its application in Pb 2 + removal. *Journal of Environmental Chemical Engineering*, 8(5), 104198. https://doi.org/10.1016/j.jece.2020.104198

(2025); www.mocedes.org/ajcer